GPS Solut (2012) 16:353–362
DOI 10.1007/s10291-011-0237-5

ORIGINAL ARTICLE

Real-time cycle slip detection in triple-frequency GNSS

Maria Clara de Lacy · Mirko Reguzzoni · Fernando Sansò

Received: 23 November 2010 / Accepted: 18 July 2011 / Published online: 9 August 2011

Abstract The modernization of the global positioning system and the advent of the European project Galileo will lead to a multifrequency global navigation satellite system (GNSS). The presence of new frequencies introduces more degrees of freedom in the GNSS data combination. We define linear combinations of GNSS observations with the aim to detect and correct cycle slips in real time. In particular, the detection is based on five geometry-free linear combinations used in three cascading steps. Most of the jumps are detected in the first step using three minimum-noise combinations of phase and code observations. The remaining jumps with very small amplitude are detected in the other two steps by means of two-tailored linear combinations of phase observations. Once the epoch of the slip has been detected, its amplitude is estimated using other linear combinations of phase observations. These combinations are defined with the aim of discriminating between the possible combinations of jump amplitudes in the three carriers. The method has been tested on simulated data and 1-second triple-frequency undifferenced GPS data coming from a friendly multipath environment. Results show that the proposed method is able to detect and repair all combinations of cycle slips in the three carriers.

M. C. de Lacy (✉)
Departamento Ingeniería Cartográfica, Geodésica y Fotogrametría, Universidad de Jaén, Jaén, Andalusia, Spain
e-mail: mclacy@ujaen.es

M. Reguzzoni
DIIAR, Politecnico di Milano, Milan, CO, Italy
e-mail: mirko.reguzzoni@polimi.it

F. Sansò
DIIAR, Politecnico di Milano, Polo Regionale di Como, Milan, CO, Italy
e-mail: fernando.sanso@polimi.it

Keywords Triple-frequency GNSS · Cycle slips · Minimum-noise combinations

Introduction

A cycle slip is a discontinuity of an integer number of cycles in the phase observable, caused by a temporary loss of lock in the receiver carrier tracking loop. This discontinuity is generally due to poor reception, or to the presence of obstacles in the path of satellite signals; its amplitude varies from one to millions of cycles.

Cycle slip detection and correction is an important part of GPS data processing. Therefore, algorithms specifically dedicated to cycle slip analysis in dual-frequency GPS observations were developed and implemented. Methods to detect and repair cycle slips using double differenced observations can be found in Bisnath and Langley (2000), Kim and Langley (2001) and Lee et al. (2003). Over the recent years, Precise Point Positioning (PPP) methods have become a powerful tool for estimating station positions. Therefore, techniques to detect and correct cycle slips on undifferenced observations are needed. The first technique to detect cycle slips on undifferenced observations was the approach called Turbo Edit (Blewitt 1990). It is implemented in scientific programs that process undifferenced observations such as GIPSY-OASIS II (Lichten et al. 1995) and BERNESE 5.0 (Beutler et al. 2006). Lacy et al. (2008) faced the cycle slip problem for single GNSS receivers by exploiting Bayesian theory. The method is based on the original signal and can be modeled by a multiple polynomial regression. Banville and Langley (2010) developed a method for instantaneous cycle slip correction in real-time PPP applications. Liu (2011) has presented a method to detect and repair cycle

slips that employs the ionospheric total electron content rate (TECR).

The space vehicles of the forthcoming GNSS satellite constellations will add additional frequencies and therefore making new linear combinations of observations available. Recently, several authors have proposed new combinations that can be used to eliminate or mitigate individual sources of error (Richert and El-Sheimy 2007). New combinations are used to face different problems. For instance, all possible triple-frequency geometry-free carrier phase combinations that retain the integer nature of the ambiguities are studied in Cocard et al. (2008). The ambiguity resolution problem in this new context is analyzed in several works (Teunissen and Odijk 2003; Ji et al. 2007; Feng 2008; Feng and Rizos 2009; Li et al. 2010). The ionosphere modeling in studied by optimal ionosphere-free combinations for triple-frequency GPS observations in Odijk (2003). Finally, some methods have developed to deal with cycle slips from a multifrequency point of view. For example, Zhen et al. (2008) presented a real-time algorithm to determine cycle slips for triple-frequency GNSS data which can be applied in PPP data processing. Dai et al. (2009) developed a real-time algorithm to detect, determine and validate cycle slips for triple-frequency GPS applying two geometry-free phase combinations along with LAMBDA technique to search for cycle slip candidates.

We present a new method for cycle slip analysis based on linear combinations of triple-frequency undifferenced GNSS observations. Section 2 describes the multifrequency GNSS observation equations. In Sect. 3, the approaches for detection of cycle slip epochs and the determination of slip amplitudes are illustrated. Section 4 describes numerical experiments to assess the performance of the method. The data consists of simulated and real 1-second triple-frequency GPS data that seem to be free of strong multipath variations since the pseudorange code noises are close to 15 cm for the first and second carrier and 10 cm for third one for all observation session. The procedure could be also used with Galileo observations; in this case, the approach should be much easier due to the lower nominal noise level of code observations, as outlined at the end of this study.

Multifrequency GNSS observation equations

The modernization of the GPS and the advent of the Galileo system will lead to a multifrequency GNSS system improving the performance of precise positioning applications. Details of the satellite constellation and frequencies for the modernized GPS and the future Galileo can be found in IS-GPS-200 (2010), IS-GPS-705 (2010) and OS SIS ICD (2010). Table 1 summarizes the modernized GPS and Open Service Galileo signal frequencies.

Table 1 Basic GPS (L) and Galileo (E) signal frequencies

Carrier	Frequency (MHz)	Wavelength (m)
L1	1,575.42	0.190
L2	1,227.60	0.244
L5	1,176.45	0.254
E2-L1-E1	1,575.42	0.190
E5b	1,207.14	0.248
E5a	1,176.45	0.254

Euler and Goad (1991) assumed some simplifications in a general model of GPS observables in order to express them in a more suitable form. These consist in writing the observables as the sum of dispersive and non-dispersive terms. Taking these simplifications into account and omitting the indices related to receiver and satellite, the mathematical model of GNSS undifferenced carrier phase and pseudorange observables for a specific receiver and satellite at epoch t is the following:

$$\begin{aligned} P_i(t) &= D(t) + k_{1i}I(t) + \varepsilon_P(t) \\ L_i(t) &= D(t) - k_{1i}I(t) + B_i + \varepsilon_L(t) \end{aligned} \tag{1}$$

where $i = 1,2,3$. The symbols P_i and L_i are the code pseudoranges and the carrier phase observations expressed in distance units at frequency f_i, respectively; ε_P and ε_L are the corresponding measurement noise, including the multipath effect. All parameters in the above equations are generally biased. The term D is the non-dispersive delay. It is interpreted as the distance traveled by the signal and is biased by clock terms and the tropospheric delay. The ionospheric group delay I at frequency f_1 is explicitly accounted for in (1) and it is multiplied by $k_{1i} = (f_1/f_i)^2$ to get the corresponding delay at frequency f_i. It is a dispersive delay biased by the Differential Code Biases (DCB). The term B_i is formed by joining the non-zero initial phase and the integer carrier phase ambiguity N_i, i.e., the initial carrier phase ambiguity at frequency f_i is biased by initialization constants and generally is not an integer. Furthermore, both equations (1) are known to be biased by the travel time of the signal through the circuitries of the receiver and satellite.

The proposed method

The problem of cycle slip detection and correction can be reduced to finding discontinuities in a noisy time series of a regularly sampled smooth signal. The processed time series are here linear combinations of phase observations, denoted as L_1, L_2, L_3 and expressed in range units, and code pseudorange observations denoted as P_1, P_2, P_3. The GPS

observations are assumed to have the realistic noise of $\sigma_{L_1} = \sigma_{L_2} = \sigma_{L_3} = 0.002$ m, $\sigma_{P_1} = \sigma_{P_2} = 0.15$ m and $\sigma_{P_3} = 0.10$ m. The respective carrier wavelengths are $\lambda_1 \approx 19.0$ cm, $\lambda_2 \approx 24.4$ cm and $\lambda_3 \approx 25.5$ cm. The integer cycle slip amplitudes are denoted as δN_1, δN_2, δN_3.

Epoch detection procedure

The proposed method is based on five linear combinations of GNSS code and phase observations used in three cascading steps. In the first one, the phase and code observations are combined to detect "big" jumps, i.e., with amplitudes much higher than the data combination noise. After that GNSS phase observations are used to detect "small" cycle slips. Finally, a further linear combination of phase observations is considered to look for the remaining undetected discontinuities.

Big jumps

The phase and code observations are combined in a minimum-noise, geometry-free combination:

$$Y_i(t) = a_{ii}L_i(t) + b_{i1}P_1(t) + b_{i2}P_2(t) + b_{i3}P_3(t) \tag{2}$$

where the coefficients are $a_{ii} = 1$, $b_{i1} = b_{i2} = -4/17$ and $b_{i3} = -9/17$ for all $i = 1,2,3$. Such coefficients are derived by imposing the following conditions:

$$\begin{cases} a_{ii} = 1 \\ a_{ii} + b_{i1} + b_{i2} + b_{i3} = 0 \\ \min\limits_{b_{i1},b_{i2},b_{i3}} \left[a_{ii}^2\sigma_{L_i}^2 + b_{i1}^2\sigma_{P_1}^2 + b_{i2}^2\sigma_{P_2}^2 + b_{i3}^2\sigma_{P_3}^2\right] \end{cases}. \tag{3}$$

Applying the covariance propagation law, the noise standard deviation (STD) of Y_i, denoted by σ_{Y_i}, is at the 7 cm level. The condition $a_{ii} = 1$ acts as a normalization condition, avoiding the amplification of unmodeled bias terms (Teunissen and Bakker 2009). Substituting (1) into (2), the combinations Y_1, Y_2, Y_3 can be expressed as the sum of the initial ambiguities, the ionospheric effect I multiplied by constants M_i and random noise. The constants M_i are given by

$$M_i = -K_{1i}a_{ii} + b_{i1} + K_{12}b_{i2} + K_{13}b_{i3} \tag{4}$$

and equal -2.57, -3.22 and -3.36 for $i = 1,2,3$, respectively. The main advantage of the combinations (2) is that simultaneous cycle slips on different carriers are not mixed and therefore, a "big" jump in one carrier cannot be compensated by jumps on the others.

The cycle slip detection test is based on the computation of the time differences ΔY_{i} between two consecutive epochs of Y_i. In particular, ΔY_{i} is considered a random variable with non-constant mean $\delta N_i\lambda_i$, which is different from zero in case of a cycle slip, and with variance depending on the noise STD σ_{Y_i} and on the ionospheric variation between two consecutive epochs.

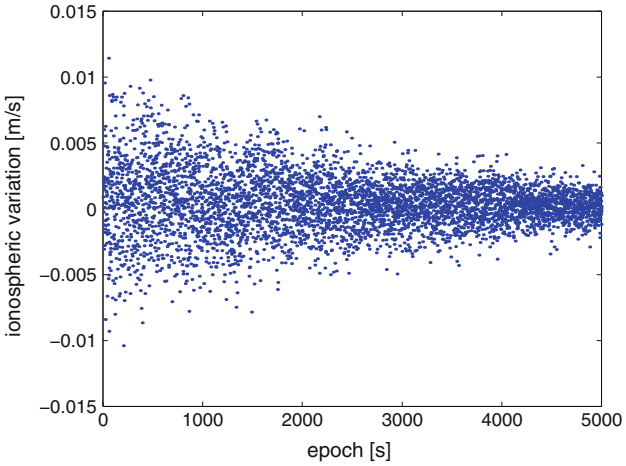

Fig. 1 An example of ionospheric effect variation in time. Station: Como (Italy). Receiver/antenna: TPS ODYSSEY-E/TPSCR3_GGD CONE. Day: 2007-12-2

Figure 1 shows a typical real example of the variation in time of the ionospheric effect ΔI. It has been computed from the function $(L_1 - L_2)/(k_{12} - 1)$. This figure is based on 1-second dual-frequency GPS data obtained from a GPS station located at Como (Italy). The receiver and antenna placed at Como are TPS ODYSSEY-E and TPSCR3_GGD CONE, respectively. GPS data correspond to the day December 2, 2007. The maximum value is at 1 cm level. The corresponding histogram is shown in Fig. 2, indicating a normal distribution with mean zero and STD of about 3 mm/s. These values prove the low impact of the ionospheric effect in differences in time of Y_i under general atmospheric conditions.

Assuming that the measurement noise is independent in time and considering ΔI as a random variable with zero mean and STD $\sigma_{\Delta I} = 3$ mm and is independent from the measurement noise, the variance of ΔY_i is

$$\sigma_{\Delta Y_i}^2 = 2\sigma_{Y_i}^2 + M_i^2\sigma_{\Delta I}^2. \tag{5}$$

It turns out that $\sigma_{\Delta Y_i}^2 \cong 10$ cm for $i = 1,2,3$.

In order to be strongly conservative, a first threshold is chosen at the level of $4\sigma_{\Delta Y_i}$. Assuming that ΔY_{i} is normally distributed around its mean value $\delta N_i\lambda_i$, the hypothesis

$$H_0 : \delta N_i = 0 \tag{6}$$

is rejected, i.e., a cycle slip is detected, if

$$\Delta Y_i(t) = |Y_i(t) - Y_i(t-1)| > 4\sigma_{\Delta Y_i} \approx 41\,\mathrm{cm} \tag{7}$$

with a significance level $\alpha = P(|Z| > 4) = 0.006\%$. The probability of "false alarms" is therefore extremely low.

On the other hand, when H_0 is not rejected, this does not mean that there are no cycle slips. A alternative hypothesis

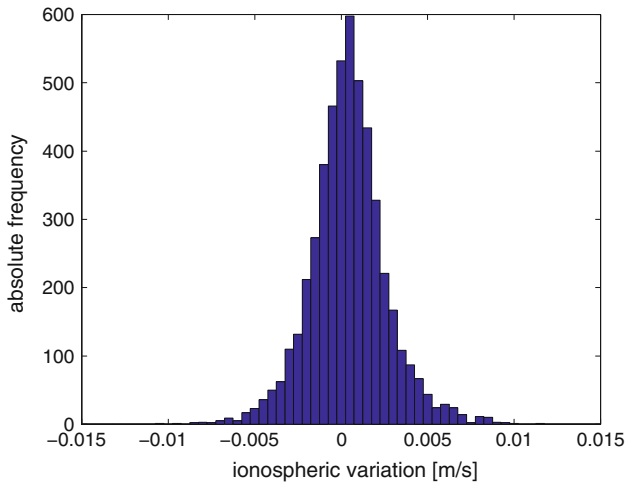

Fig. 2 Histogram of the time variation of the ionospheric effect of data from Fig. 1

test is setup by computing, for different integer values $\delta N_i > 0$, the probability of missed detection as

$$\beta = P\left(Z > \frac{\delta N_i \lambda_i - 4\sigma_{\Delta Yi}}{\sigma_{\Delta Yi}}\right) \tag{8}$$

i.e., the probability that H_0 is incorrectly not rejected when actually $\delta N_i \neq 0$ (Fig. 3).

The amplitude of cycle slips in Y_1, Y_2, Y_3 for δN_1, δN_2, δN_3 varying from 1 to 5 (higher slips are surely detected) is shown in Fig. 4. It turns out that only the cycle slips represented by dots in Fig. 4 have a probability $\beta < 0.01\%$ that we consider acceptable; this limit value of β is computed from (8) for $i = 2$ and $\delta N_2 = 3$. The other cycle slips, corresponding to the cases $|\delta N_1| = 1, 2, 3, |\delta N_2| = 1, 2$ and $|\delta N_3| = 1, 2$, are called from here on "small jumps" and are represented by stars in Fig. 4. They are considered non-detectable by the combinations (2) and therefore have to be submitted to a further testing procedure.

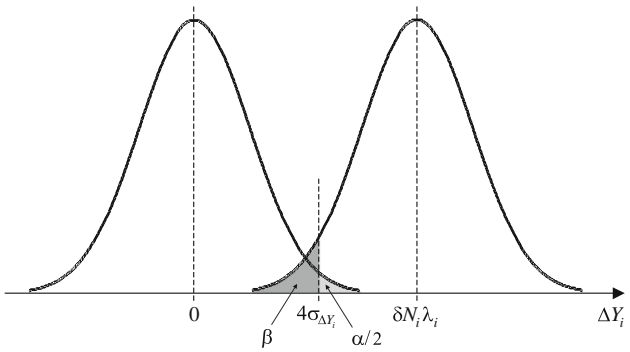

Fig. 3 Significance level α and risk of second kind β for cycle slip detection tests on ΔY_1, ΔY_2 and ΔY_3

Small jumps

In order to detect the remaining small jumps, the noise level of the data combination has to be reduced. This is done by combining only GPS phase observations in a geometry-free and ionosphere-free linear combination:

$$Y_4(t) = a_{41}L_1(t) + a_{42}L_2(t) + a_{43}L_3(t) \tag{9}$$

with $a_{41} = 14/65$, $a_{42} = -79/65$ and $a_{43} = 1$, derived from the following conditions:

$$\begin{cases} a_{43} = 1 \\ a_{41} + a_{42} + a_{43} = 0 \\ a_{41} + K_{12}\, a_{42} + K_{13} a_{43} = 0 \end{cases}. \tag{10}$$

The resulting noise STD σ_{Y_4} is at the 3 mm level, much lower than the one of combinations (2).

Since Y_4 is an ionosphere-free combination and assuming again that the measurement noise is independent in time, the variance of the time variation ΔY_4 can be simply computed as:

$$\sigma^2_{\Delta Y_4} = 2\sigma^2_{Y_4} \tag{11}$$

Moreover, assuming that ΔY_4 is normally distributed, the hypothesis

$$H_0 : \delta N_1 = \delta N_2 = \delta N_3 = 0 \tag{12}$$

is rejected, i.e., a cycle slip is detected, if

$$\Delta Y_4(t) = |Y_4(t) - Y_4(t-1)| > 4\sigma_{\Delta Y_4} \approx 1.8\,\text{cm} \tag{13}$$

with a significance level $\alpha = 0.006\%$.

The values of the jumps in Y_4 for all the possible combinations of three cycle slips that are not yet detectable are shown in Fig. 5. The number of slip combinations (δN_1, δN_2, δN_3) under test, for $|\delta N_1| \leq 3$, $|\delta N_2| \leq 2$, $|\delta N_3| \leq 2$ and

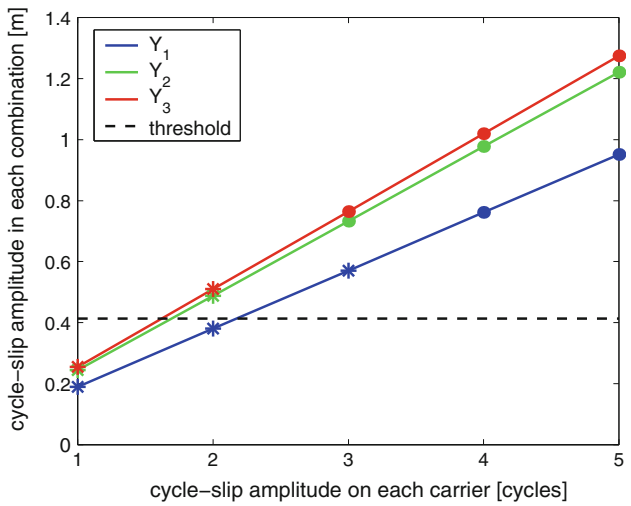

Fig. 4 Certainly detected (*dots*) and possibly undetected (*stars*) cycle slips by ΔY_1, ΔY_2 and ΔY_3 using the threshold in *dash line*

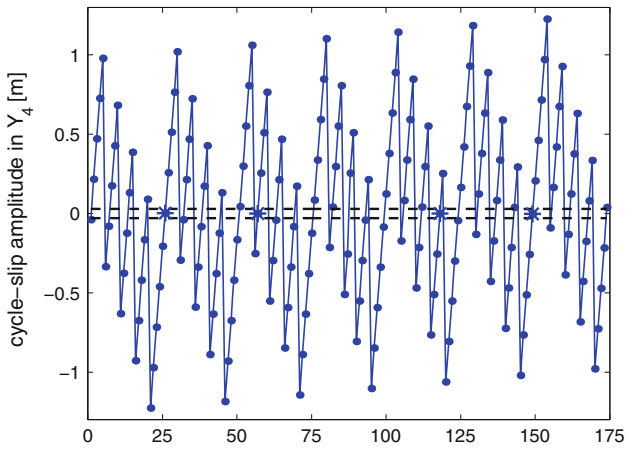

Fig. 5 Detected (*dots*) and undetected (*stars*) cycle slips by ΔY_4. Threshold in *dash line*

excluding the no-slip case (0, 0, 0), is equal to $7\times5\times5-1=174$. The only slip combinations that are not seen by ΔY_4 are (−2, −2, −2), (−1, −1, −1), (+1,+1,+1) and (+2, +2, +2), i.e., simultaneous cycle slips with the same amplitude in all three carriers ($\delta N_1 = \delta N_2 = \delta N_3 = -2, -1, 1, 2$). Note that $\beta \approx 0$ for all other detected cycle slips.

Particular cases

In order to deal with the undetected cycle slips ($\delta N_1 = \delta N_2 = \delta N_3 = \delta N$), a tailored linear combination of phase observations is finally introduced:

$$Y_5(t) = a_{51}L_1(t) + a_{52}L_2(t) + a_{53}L_3(t) \tag{14}$$

with $a_{51} = 1, a_{52} = 0.37$ and $a_{53} = -0.63$. This is a geometry-free combination that maximizes the ratio between the squared amplitude of the smallest jump, corresponding to $|\delta N_1| = 1$, and the variance of the time differences ΔY_5:

$$\begin{cases} a_{51} = 1 \\ a_{51} + a_{52} + a_{53} = 0 \\ \max\limits_{a_{52},a_{53}} \left[\frac{(a_{51}\lambda_1 + a_{52}\lambda_2 + a_{53}\lambda_3)^2}{\sigma^2_{\Delta Y_5}} \right] \end{cases} \tag{15}$$

where

$$\sigma^2_{\Delta Y_5} = 2\sigma^2_{Y_5} + M_5^2\sigma^2_{\Delta I} \tag{16}$$

$$\sigma^2_{Y_5} = a^2_{51}\sigma^2_{L_1} + a^2_{52}\sigma^2_{L_2} + a^2_{53}\sigma^2_{L_3} \tag{17}$$

$$M_5 = a_{51} + K_{12}a_{52} + K_{13}a_{53}. \tag{18}$$

The resulting noise STD σ_{Y_5} is at the 2.5 mm level. Therefore, since a cycle slip equal to (+1, +1, +1) produces a jump of 8 cm, all cycle slips with the same amplitude in the three carriers should be detected if the ionosphere variation between two consecutive epochs is less than 7 cm, which is a very high value under general atmospheric conditions.

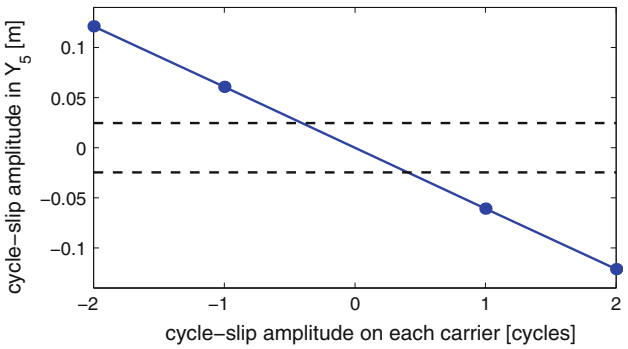

Fig. 6 Detected cycle slips (*dots*) by ΔY_5. Threshold in *dash line*

More precisely, observing that $\sigma_{\Delta Y_5} \approx 4$ mm and assuming that ΔY_5 is normally distributed, the hypothesis

$$H_0 : \delta N = 0 \tag{19}$$

is rejected, i.e., a cycle slip is detected, if

$$\Delta Y_5(t) = |Y_5(t) - Y_5(t-1)| > 4\sigma_{\Delta Y_5} \approx 1.7\,\text{cm} \tag{20}$$

with a significance level $\alpha = 0.006\%$. Figure 6 shows that all the analyzed cycle slips have an amplitude in Y_5 that allows their detection. In addition, $\beta \approx 0$ for all of them.

Amplitude determination procedure

Once the epoch has been detected, the problem is to estimate the amplitude of the jump, i.e., the integer number of cycles slipped in each of these carriers. In the proposed method, the cycle slip amplitude estimation is based on linear combinations of phase observations. A rough estimate of the cycle slip amplitudes can be computed as:

$$\delta\tilde{N}_i = \text{round}\left(\frac{\Delta Y_i}{\lambda_i}\right) \tag{21}$$

with $i = 1, 2, 3$.

By comparing the carrier wavelengths with the noise level of ΔY_i ($\sigma_{\Delta Y_i} \approx 10$ cm), we can state that the true cycle slip amplitudes are in the range of $\delta N_i = \delta\tilde{N}_i + \delta n_i$ with $\delta n_i = -2, -1, 0, +1, +2$. In order to determine the correct values, we consider the phase combinations

$$\begin{aligned} L_{12}(t) &= L_1(t) - L_2(t) \\ L_{13}(t) &= L_1(t) - L_3(t) \end{aligned} \tag{22}$$

and their differences in time

$$\begin{aligned} \Delta L_{12}(t) &= L_{12}(t) - L_{12}(t-1) \\ \Delta L_{13}(t) &= L_{13}(t) - L_{13}(t-1). \end{aligned} \tag{23}$$

The selected cycle slip amplitudes with respect to δn_i are those minimizing the following target functions

$$\phi_{12}(t) = \left|\Delta L_{12}(t) - (\delta\tilde{N}_1\lambda_1 - \delta\tilde{N}_2\lambda_2) - (\delta n_1\lambda_1 - \delta n_2\lambda_2)\right|$$
$$\phi_{13}(t) = \left|\Delta L_{13}(t) - (\delta\tilde{N}_1\lambda_1 - \delta\tilde{N}_3\lambda_3) - (\delta n_1\lambda_1 - \delta n_3\lambda_3)\right|. \quad (24)$$

The question is whether these target functions are robust enough to discriminate among all possible 125 combinations of cycle slip amplitudes that include the case of no-slip. The answer is positive only if the following two conditions

$$\frac{1}{2}D_{12}(\delta n_1, \delta n_2, \delta m_1, \delta m_2) > 4\sigma_{\Delta L_{12}}$$
$$\frac{1}{2}D_{13}(\delta n_1, \delta n_3, \delta m_1, \delta m_3) > 4\sigma_{\Delta L_{13}} \quad (25)$$

with

$$D_{12}(\delta n_1, \delta n_2, \delta m_1, \delta m_2) = \left|(\delta n_1\lambda_1 - \delta n_2\lambda_2) - (\delta m_1\lambda_1 - \delta m_2\lambda_2)\right|$$
$$D_{13}(\delta n_1, \delta n_3, \delta m_1, \delta m_3) = \left|(\delta n_1\lambda_1 - \delta n_3\lambda_3) - (\delta m_1\lambda_1 - \delta m_3\lambda_3)\right| \quad (26)$$

are both verified for all $\delta n_i, \delta m_i = -2, -1, 0, +1, +2$ such that $(\delta n_1, \delta n_2) \neq (\delta m_1, \delta m_2)$ and $(\delta n_1, \delta n_3) \neq (\delta m_1, \delta m_3)$. In this case, the semi-distance between any two points in the lattice $(\delta n_1, \delta n_2, \delta n_3)$ with $\delta n_i = -2, -1, 0, +1, +2$ is larger than 4σ. The implication is that the selected minimum of (24) cannot have an alternative with a reasonable probability, i.e., the probability of a wrong decision is $P(Z > 4) = 0.003\%$. If both conditions (25) are verified, we can reasonably state that the noise of the phase observations cannot bias the amplitude estimation.

The result for the first condition (25) is shown in Fig. 7: the only two uncertain cases of $(\delta n_1, \delta n_2)$ with a semi-distance in L_{12} below the threshold are as follows:

- $(-2, -2)$ that could be confused with $(+2, +1)$
- $(-2, -1)$ that could be confused with $(+2, +2)$

The same uncertain cases can be found for $(\delta n_1, \delta n_3)$ as a consequence of the close values of λ_2 and λ_3.

If the uncertainty is just in one of the two target functions (24), then the value of δn_1 can be determined and can be used to solve the uncertainty in the other target function, i.e., the only cases of $(\delta n_1, \delta n_2, \delta n_3)$ that cannot be discriminated by combining the two target functions are as follows:

- $(-2, -2, -2)$ versus $(+2, +2, +1)$
- $(-2, -1, -2)$ versus $(+2, +2, +1)$
- $(+2, +1, +2)$ versus $(-2, -2, -1)$
- $(+2, +2, +2)$ versus $(-2, -1, -1)$

Therefore, a final combination

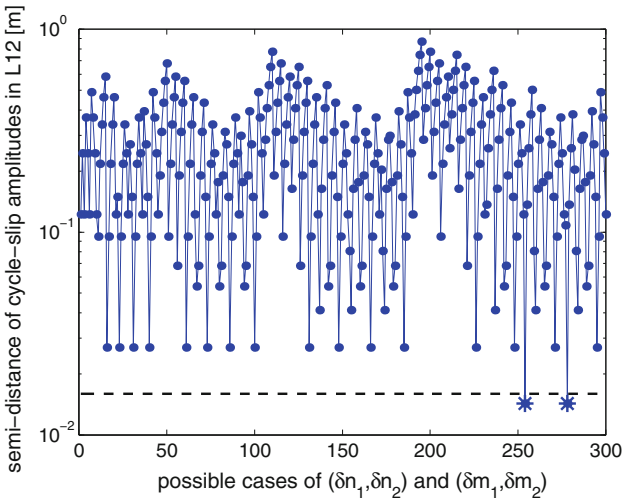

Fig. 7 Uncertain cycle slip amplitudes (*stars*) with a semi-distance $\frac{1}{2}D_{12}(\delta n_1, \delta n_2, \delta m_1, \delta m_2)$ smaller than the 4σ threshold (*dash line*). The minimization of the target function $\phi_{12}(t)$ is not decisive to discriminate between them

$$Y_6(t) = a_{61}L_1(t) + a_{62}L_2(t) + a_{63}L_3(t) \quad (27)$$

is introduced with $a_{61} = 1, a_{62} = -2.78$ and $a_{63} = -1.78$. Observing that the absolute difference between two cycle slip amplitudes in Y_6 is the same for all four cases mentioned before, i.e., it is equal to

$$d_6 = |4a_{61}\lambda_1 + 3a_{62}\lambda_2 + 3a_{63}\lambda_3|. \quad (28)$$

The coefficients of the linear combination (27) are derived by imposing the following conditions:

$$\begin{cases} a_{61} = 1 \\ a_{61} + a_{62} + a_{63} = 0 \\ \max\limits_{a_{62}, a_{63}} \left[\frac{d_6^2}{\sigma^2_{\Delta Y_6}}\right] \end{cases} \quad (29)$$

where

$$\sigma^2_{\Delta Y_6} = 2\sigma^2_{Y_6} + M_6^2\sigma^2_{\Delta I} \quad (30)$$
$$\sigma^2_{Y_6} = a^2_{61}\sigma^2_{L_1} + a^2_{62}\sigma^2_{L_2} + a^2_{63}\sigma^2_{L_3} \quad (31)$$
$$M_6 = a_{61} + K_{12}a_{62} + K_{13}a_{63}. \quad (32)$$

This means that Y_6 is a geometry-free combination that maximizes the ratio of the squared difference between two uncertain cycle slips and the variance of the data time variations. The resulting noise STD σ_{Y_6} is close to 1 cm.

At this point, the following target function to be minimized is defined

$$\phi_6(t) = \left|\Delta Y_6(t) - \left(a_{61}\delta\tilde{N}_1\lambda_1 + a_{62}\delta\tilde{N}_2\lambda_2 + a_{63}\delta\tilde{N}_3\lambda_3\right) - (a_{61}\delta n_1\lambda_1 + a_{62}\delta n_2\lambda_2 + a_{63}\delta n_3\lambda_3)\right| \quad (33)$$

which is capable of solving the remaining uncertainty on $(\delta n_1, \delta n_2, \delta n_3)$, because the semi-distance between two uncertain cases in Y_6 is in the order of $3\sigma_{\Delta Y_6}$. This is slightly less conservative than conditions (25), but it is acceptable also because there is a very low probability getting at this final test.

Application to the case of Galileo

The expected nominal noise level of the Galileo code pseudorange observations is lower than that for the modernized GPS. In particular, in case of Galileo, we are expected to have $\sigma_{P_1} = 0.07\,\text{m}$ and $\sigma_{P_2} = \sigma_{P_3} = 0.04\,\text{m}$ (O'Keefe et al. 2005, B. Arbesser-Rastburg, personal communication).

As a consequence of the STD of these pseudorange observations, the noise STD of the combinations Y_1, Y_2, Y_3 becomes $\sigma_{Y_1} = 2.6\,\text{cm}$. This means that, in principle, the presence and the amplitude of cycle slips on L_2 and L_3 can be directly detected by using Y_2 and Y_3, respectively. In the case of L_1, we need also the combination Y_4 to identify slips of one cycle only; since the amplitude estimated by Y_1 has an uncertainty of ± 1, we can determine the right number of integer cycles slipped on L_1 with the support of L_{12} or L_{13}. It is clear that the procedure is much easier in case of Galileo, provided that this nominal accuracy is confirmed with real data in the future.

Numerical tests

The capability of the method to detect and repair cycle slips has been tested in two different situations: simulated data with cycle slips and real triple-frequency GPS data with artificial cycle slips.

Simulated data

The performance of the proposed method is assessed by simulated data first. A time series of 5,000 values is considered with a known jump equal to $(0, -1, -1)$ at epoch $\tau = 1,250$. The ionospheric effect is simulated by using $L_1 - L_2$ observations coming from 1-second real GPS data. The resulting signal in Y_1, Y_2 and Y_3 is shown in Fig. 8. It can be seen that the discontinuity is quite embedded into these linear combinations and cannot be detected by time differentiation (Fig. 9). On the other hand, the jump is clearly revealed in Y_4 thanks to the improved signal-to-noise ratio (Fig. 10). Figure 11 shows the values of differencing Y_4 in time. The linear combination Y_5 is displayed in Fig. 12 for the sake of completeness, but it is not used in the cycle slip epoch detection.

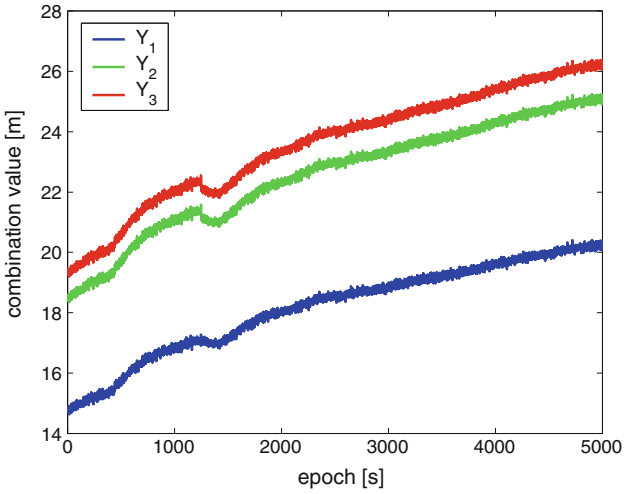

Fig. 8 Linear combinations Y_1, Y_2 and Y_3

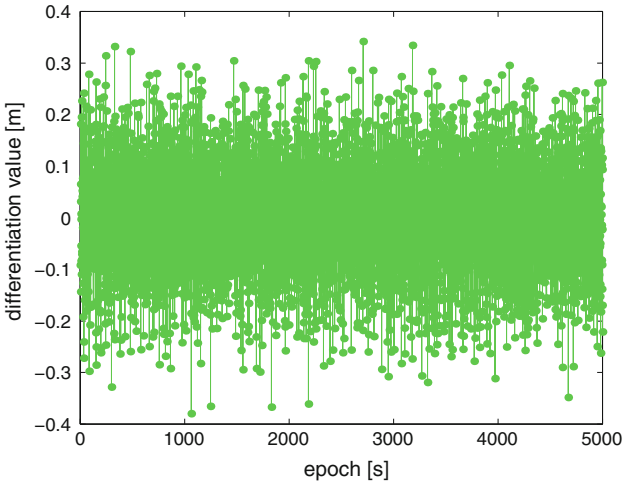

Fig. 9 Differentiation of Y_2 in time (ΔY_2). Similar behavior for Y_1 and Y_3

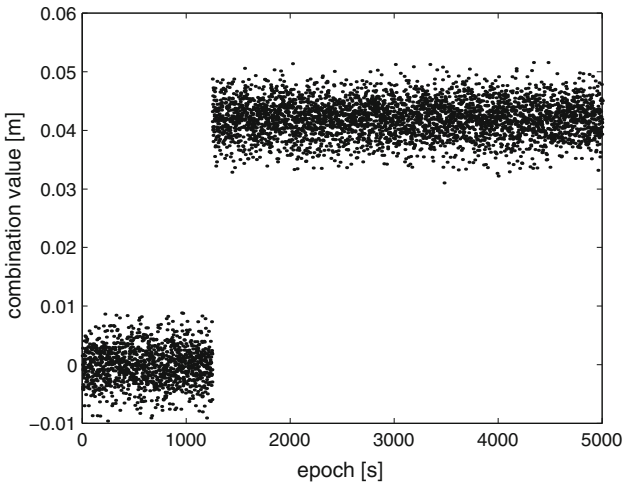

Fig. 10 Linear combination Y_4

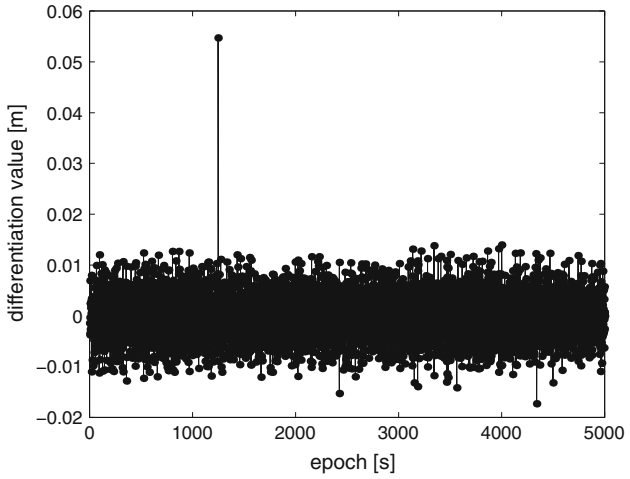

Fig. 11 Differentiation of Y_4 in time (ΔY_4)

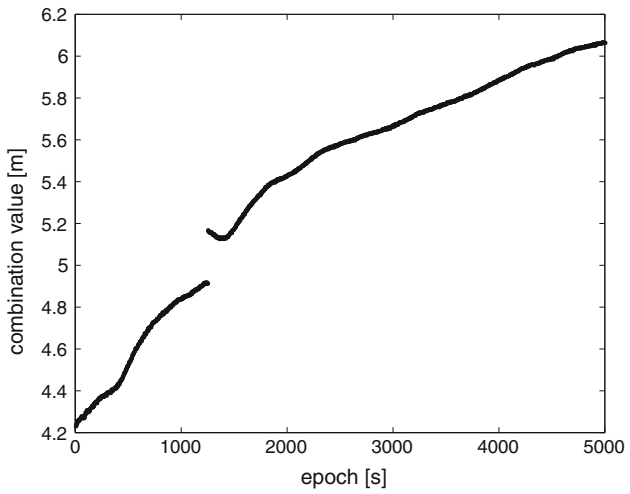

Fig. 12 Linear combination Y_5

From the numerical point of view, the results of the tests (7), (13), (20) are as follows:

- $\Delta Y_1(\tau) = 30.3$ cm > 41.3 cm
- $\Delta Y_2(\tau) = 4.4$ cm > 41.4 cm
- $\Delta Y_3(\tau) = 4.3$ cm > 41.4 cm
- $\Delta Y_4(\tau) = 5.5$ cm > 1.8 cm
- $\Delta Y_5(\tau) = 26.0$ cm > 1.7 cm

This means that the jump is detected by Y_4 at the correct epoch $\tau = 1,250$.

Regarding the amplitude estimation, the initial estimates are $\delta\tilde{N}_1 = 2$, $\delta\tilde{N}_2 = 0$ and $\delta\tilde{N}_3 = 0$ according to (21). Considering a range of ± 2 around these estimates, the minima of the target functions (24) are as follows:

- $\min[\phi_{12}(\tau)] = 1.4$ cm for $(\delta n_1, \delta n_2) = (+2, +2)$
- $\min[\phi_{13}(\tau)] = 1.3$ cm for $(\delta n_1, \delta n_3) = (+2, +2)$

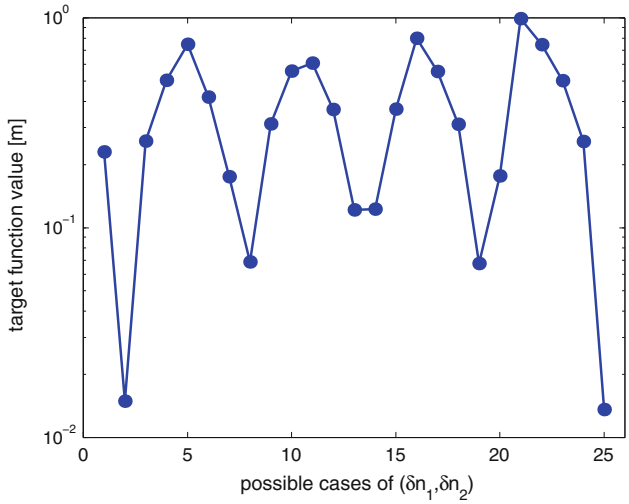

Fig. 13 Values of the target function $\phi_{12}(\tau)$ for all possible cases of $(\delta n_1, \delta n_2)$. The cycle slip amplitude in L_{12} is uncertain, because the two smallest values of $\phi_{12}(\tau)$ are very similar: $\phi_{12}(\tau) = 1.5$ cm for $(\delta n_1, \delta n_2) = (-2, -1)$, $\phi_{12}(\tau) = 1.4$ cm for $(\delta n_1, \delta n_2) = (+2, +2)$

corresponding to the uncertain case $(\delta n_1, \delta n_2, \delta n_3) = (+2, +2, +2)$ that can be confused with $(-2, -1, -1)$, as explained in Sect. 3.2 and shown in Fig. 13.

Testing the two alternatives by using the target function (33), the corresponding values are

- $\phi_6(\tau) = 5.4$ cm for $(\delta n_1, \delta n_2, \delta n_3) = (+2, +2, +2)$
- $\phi_6(\tau) = 3.2$ cm for $(\delta n_1, \delta n_2, \delta n_3) = (-2, -1, -1)$

and therefore the estimated $(\delta n_1, \delta n_2, \delta n_3)$ is modified to $(-2, -1, -1)$. Recalling that $\delta\hat{N}_i = \delta\tilde{N}_i + \delta n_i$, the final estimate of the cycle slip amplitude is $(\delta\hat{N}_1, \delta\hat{N}_2, \delta\hat{N}_3) = (0, -1, -1)$ which corresponds to the true one.

The method has been tested on 1,000 cases by adding cycles slips at random positions and with random amplitudes. All the cases have been correctly detected.

Real triple-frequency GPS data

In order to evaluate the performance of the method with real data, artificial jumps have been added to 1-second triple-frequency GPS data taken from ftp://cddis.gsfc.nasa.gov/pub/gps/data. In particular, data corresponding to the day 2011-02-28 taken from the station of WTZZ (Wettzell, Germany) are considered. Only satellite PRN1 has triple-frequency GPS data therefore only this satellite is considered. The noise of the pseudoranges in this data set is close to the values assumed in our method. This is 16 cm level for the first one, 17 cm for the second one and 10 cm for the third one. First, our program was used on this data set and no cycle slips were detected. Then, some artificial jumps were added to be sure that the program detects the correct epoch and estimates the correct amplitude, since the

Table 2 Artificial cycle slips in real GPS data

True epoch	True amplitude	Estimated epoch	Jump class	Difference in time (m)	Estimated amplitude
57	(1, 1, 1)	57	Particular case	$\Delta Y_5 = -0.084$	(1, 1, 1)
152	(2, 2, 2)	152	Particular case	$\Delta Y_5 = -0.159$	(2, 2, 2)
332	(1, 0, 1)	332	Small	$\Delta Y_4 = 0.291$	(1, 0, 1)
392	(0, 0, 1)	392	Small	$\Delta Y_4 = 0.248$	(0,0,1)
408	(3, 3, 3)	408	Big	$\Delta Y_1 = 0.591$	(3, 3, 3)
				$\Delta Y_2 = 0.752$	
				$\Delta Y_3 = 0.784$	
408	(3, 3, 2)	408	Big	$\Delta Y_1 = 0.591$	(3, 3, 2)
				$\Delta Y_2 = 0.752$	
				$\Delta Y_3 = 0.520$	
408	(3, 2, 2)	408	Small	$\Delta Y_4 = 0.039$	(3, 2, 2)
511	(2, 1, 1)	511	Small	$\Delta Y_4 = 0.041$	(2, 1, 1)
511	(1, −1, 0)	511	Small	$\Delta Y_4 = 0.339$	(1, −1, 0)
515	(5, 5, 5)	515	Big	$\Delta Y_1 = 0.992$	(5, 5, 5)
				$\Delta Y_2 = 1.260$	
				$\Delta Y_3 = 1.314$	
517	(3, 2, 2)	517	Big	$\Delta Y_1 = 0.682$	(3, 2, 2)
				$\Delta Y_2 = 0.600$	
				$\Delta Y_3 = 0.621$	
517	(1, 3, 2)	517	Big	$\Delta Y_1 = 0.302$	(1, 3, 2)
				$\Delta Y_2 = 0.844$	
				$\Delta Y_3 = 0.621$	
517	(−1, 0, 0)	517	Small	$\Delta Y_4 = 0.041$	(−1, 0, 0)
517	(−2, −1, −1)	517	Small	$\Delta Y_4 = -0.039$	(−2, −1, −1)
517	(0, −1, −1)	517	Small	$\Delta Y_4 = -0.042$	(0, −1, −1)

The epoch and amplitude of the jump were estimated by the proposed method

epoch and the amplitude of the jumps are known a priori. As it is shown in Table 2, all artificial jumps added in the data set are correctly detected and estimated.

We would like to mention that 30-second triple-frequency GPS data belonging to the satellite PRN25 and acquired from station UNB3 (University of New Brunswick, Canada) are also available in the above cited ftp-server. However, this data set has not been analyzed because it contains strong variations of pseudorange noise (Bakker et al. 2011) which are not expected from future modernized GPS signals.

Conclusions

Tailored linear combinations of GNSS triple-frequency observations are defined to solve cycle slip detection and correction in undifferenced GNSS observations. The method can be applied in real time because it is computationally easy and requires only comparisons between values of two consecutive epochs. The method has been tested on modernized GPS simulated data, showing that all combinations of simultaneous cycle slips in the three carriers can be detected and repaired under the considered hypothesis. Moreover, in the rare event that a false alarm happens, i.e., a cycle slip is detected but is not present in the data, a zero amplitude is always correctly estimated. Furthermore, the method has been tested on 1-second real triple-frequency GPS data with levels of pseudorange noise close to 15 cm for the first and second carrier and close to 10 cm for the third one. All artificial jumps added to real data have been correctly detected and estimated. As for the Galileo satellites, the nominal noise level of the code observations is expected to be lower than that assumed in our method. Consequently, the procedure will be even easier, requiring only a smaller number of combinations.

As to future work, the method will be checked with other programs that deal with the cycle slip problem if available. Similar linear observation combinations could be also used to deal with the problem of integer ambiguity resolution.

Acknowledgments This study has been funded by the Spanish Government through the Research Project entitled ‘‘Nuevos

algoritmos para el futuro sistema GNSS multifrecuencia'' with reference AYA2008-02948.

References

Bakker PF de, Tiberius CJM, van der Marel H, van Bree RJP (2011) Short and zero baseline analysis of GPS L1 C/A, L5Q, GIOVE E1B, and E5aQ signals. GPS Solut. doi:10.1007/s10291-011-0202-3 (published on line)

Banville S, Langley RB (2010) Instantaneous cycle slips correction for real time PPP applications. Navigation 57(4):325–334

Beutler G, Bock H, Brockmann E, Dach R, Fridez P, Gurtner W, Habrich H, Hugentobler U, Ineichen D, Jaeggi A, Meindl M, Mervart L, Rothacher M, Schaer S, Schmid R, Springer T, Steigenberger P, Svehla D, Thaller D, Urschl C, Weber R (2006) BERNESE GPS software version 5.0

Bisnath SB, Langley RB (2000) Automated cycle-slip correction of dual-frequency kinematic GPS data. In: Proceedings of 47th conference of CASI, Ottawa, Canada

Blewitt G (1990) An automatic editing algorithm for GPS Data. Geophys Res Lett 17(3):199–202

Cocard M, Bourgon S, Kamali O, Collins P (2008) A systematic investigation of optimal carrier-phase combinations for modernized triple-frequency GPS. J Geod 82:55–564. doi:10.1007/s00190-007-0201-x

Dai Z, Knedlik S, Loffeld O (2009) Instantaneous triple-frequency GPS cycle-slip detection and repair. Int J Navig Obs. Article ID 407231. doi:10.1155/2009/407231

Euler HJ, Goad CC (1991) On optimal filtering of GPS dual frequency observations without using orbit information. Bull Geodesique 65:130–143

Feng Y (2008) GNSS three carrier ambiguity resolution using ionosphere-reduced virtual signal. J Geod 82(12):847–862

Feng Y, Rizos C (2009) Network-based geometry-free three carrier ambiguity resolution and phase bias calibration. GPS Solut 13(1):43–56. doi:10.1007/s10291-008-0098-8

IS-GPS-200 (2010) Global positioning system wing (GPSW) systems engineering and integrations. Available at http://www.gps.gov/technical/icwg/

IS-GPS-705 (2010) Global positioning system wing (GPSW) systems engineering and integrations. Available at http://www.gps.gov/technical/icwg/

Ji S, Chen W, Zhao C, Ding X, Chen Y (2007) Single epoch ambiguity resolution for Galileo with the CAR and LAMBDA methods. GPS Solut 11(4):259–268

Kim D, Langley RB (2001) Instantaneous real-time cycle-slip correction of dual frequency GPS data. In: Proceedings of the international symposium on kinematic systems in geodesy, geomatics and navigation, pp 255–264

Lacy MC de, Reguzzoni M, Sansò F, Venuti G (2008). The Bayesian detection of discontinuities in a polynomial regression and its application to the cycle slip problem. J Geod 82(9):527–542

Lee HK, Wang J, Rizos C (2003) Effective cycle slip detection and identification for high precision GPS/INS integrated systems. J Navig 56(3):475–486. doi:10.1017/S0373463303002443

Li B, Feng Y, Shen Y (2010) Three carrier ambiguity resolution: distance-independent performance demonstrated using semi-generated triple frequency GPS signals. GPS Solut 14(2):177–184

Lichten SM, Bar-Sever YE, Bertiger EI, Heflin M, Hurst K, Muellerschoen RJ, Wu SC, Yunck TP, Zumberge JF (1995) GIPSY-OASIS II: a high precision GPS data processing system and general orbit analysis tool, technology 2006, NASA Technology Transfer Conference, Chicago, Illinois, 24–26 October 1995

Liu Z (2011) A new automated cycle slip detection and repair method for a single dual-frequency GPS receiver. J Geod 85:171–183. doi:10.1007/s00190-010-0426-y

Odijk D (2003) Ionosphere-free phase combinations for modernized GPS. J Survey Eng 129(4):165–173

O'Keefe K, Julien O, Cannon ME, Lachapelle G (2005) Availability, accuracy, reliability, and carrier-phase ambiguity resolution with Galileo and GPS. Acta Astronautica 58(8):422–434

OS SIS ICD (2010) European GNSS (Galileo) open service. Signal in space. Interface control document. Issue 1.1. Available at http://ec.europa.eu/enterprise/policies/satnav/galileo

Richert T, El-Sheimy N (2007) Optimal linear combinations of triple frequency carrier phase data from future global navigation satellite systems. GPS Solut 11:11–19

Teunissen PJG, Bakker PF de (2009). Next generation GNSS single receiver cycle slip reliability. Proceedings of the VII Hotine-Marussi Symposium, Rome, Italy, 6–10 July 2009. In print

Teunissen PJG, Odijk D (2003) Rank defect integer estimation and phase-only modernized GPS ambiguity resolution. J Geod 76(9–10):259–268

Zhen D, Stefan K, Otmar L (2008) Realtime cycle slip detection and determination for multiple frequency GNSS. In: Proceedings of the 5th workshop on positioning, navigation and communication 2008 (WPNC'08)